ACADEMIC PRESS

Available online at www.sciencedirect.com

SCIENCE DIRECT®

Journal of Sound and Vibration 260 (2003) 329–348

JOURNAL OF SOUND AND VIBRATION

www.elsevier.com/locate/jsvi

Simplified mobility expressions for infinite in-vacuo pipes

M.J. Brennan*, W. Variyart

Institute of Sound and Vibration Research, University of Southampton, Southampton, UK SO17 1BJ

Received 25 October 2001; accepted 18 March 2002

Abstract

In this paper, closed-form expressions for the mobility of the circumferential modes in an infinite in-vacuo thin-walled pipe are derived in terms of the axial wave receptances for each mode. These expressions are valid below the ring frequency. By using simplified expressions for the wavenumbers, low-frequency approximations for the point and transfer mobilities are also derived. These new mobility expressions are validated experimentally, and are used to examine the dynamic behaviour of an in-vacuo pipe.

1. Introduction

A convenient way to characterise the dynamic behaviour of shell structures, such as rings and pipes is by their point and transfer mobilities. For a ring, these are given in Ref. [1]. Because of different analysis approaches, the literature for pipes is split into two categories; that for finite and for infinite pipes. For finite pipes, the analysis is usually based on modal decomposition in both the circumferential and axial directions [2–4]. The analysis of infinite pipes generally employs a wave approach in the axial direction together with modal decomposition in the circumferential direction. Several researchers have performed such analyses for in vacuo [5,6], and fluid-filled pipes [7–10]. The main difference between these two situations is the number of axial waves that can exist for each circumferential mode. In in vacuo pipes, there are eight structural axial waves for each circumferential mode, whereas in fluid-filled pipes there are fluid waves in addition.

To obtain the mobilities of infinite pipes, most researchers have used the Fourier transform to transform the equations of motion into the wavenumber domain. They solve the equations using the method of residues [11], and then use the inverse Fourier transform back to the spatial

*Corresponding author. Tel.: +44-23-8059-4937; fax: +44-23-8059-3190.
E-mail address: mjb@isvr.soton.ac.uk (M.J. Brennan).

0022-460X/03/$ - see front matter
PII: S0022-460X(02)00947-1

domain. While this approach has mathematical elegance, it can mask some of the physics. Recently, Fégeant has used a perturbation method to determine the point mobility for axisymmetrically excited infinite pipes [12].

In this paper, an alternative approach is adopted to derive point and transfer mobilities for an in vacuo infinite pipe using Hooke's and Newton's laws and eight boundary conditions at the excitation point. The mobilities are decomposed into circumferential modes, and each mode is decomposed into eight axial waves, four of which are left-going and four of which are right-going. This approach enables expressions for each of the wave amplitudes to be derived for a harmonic radial point force, and by summing these wave expressions for the modal amplitudes can also be derived, which in turn, can be summed to give the total mobility. Once these expressions are established, they are simplified for low-frequency behaviour using wavenumber expressions derived by the authors in Ref. [13] to compare the dynamics of a pipe with that of simple structures such as a membrane and a beam. By decomposing the response of an infinite pipe in terms of waves, it is possible to determine the dominant waves for each circumferential mode at each frequency for both the point and transfer mobilities, thus facilitating physical insight.

To validate the expressions derived in this paper they are compared with measurements taken on a PVC pipe fitted with anechoic terminations at each end.

2. Derivation of mobility expressions

The co-ordinate system for an infinite in vacuo pipe of mid-surface radius a and wall thickness h is shown in Fig. 1(a), where w, v and u are the radial, tangential and axial pipe displacements, respectively; θ is the azimuthal angle and ϕ is a reference angle clockwise from the vertical. Because of the closure of the pipe in the circumferential direction, the mode shapes in this direction take the form of sine or cosine functions. The first four modes are illustrated in Fig. 1(b), where n denotes the modal order, which conventionally starts at $n = 0$; n also denotes the integer number of circumferential wavelengths that fit into the circumference of the pipe at the cut-on frequency of the nth mode. For each mode, eight axial waves can potentially exist at any frequency, four are right-going and four are left-going. The characteristics of these waves have been described by the authors in Ref. [13].

To investigate the dynamic behaviour of the pipe, when it is excited by a radial harmonic point force of amplitude F_0, a small element is considered. A free-body diagram depicting the forces and moments acting on the pipe element is shown in Fig. 2. Summing the resultant radial forces (expressed in units of force per unit mid-surface length of the pipe) and applying Newton's second law, gives [3]

$$-N_\theta + \frac{\partial Q_s}{\partial s} + \frac{\partial Q_\theta}{\partial \theta} - \rho a h \frac{\partial^2 w}{\partial t^2} = \frac{F_0}{a}\delta(s)\delta(\theta - \phi)\mathrm{e}^{-\mathrm{j}\omega t}, \tag{1}$$

where ρ is the density of the pipe, $s = x/a$ is the non-dimensional axial distance along the pipe, δ is the delta function, N_θ is the in-plane circumferential force, $Q_s = (1/a)(\partial M_s/\partial s + \partial M_{\theta s}/\partial \theta)$ is the axial transverse shear force, $Q_\theta = (1/a)(\partial M_\theta/\partial \theta + \partial M_{s\theta}/\partial s)$ is the circumferential transverse shear force, M_s and M_θ are the axial and circumferential bending moments, and $M_{s\theta}$ and $M_{\theta s}$ are

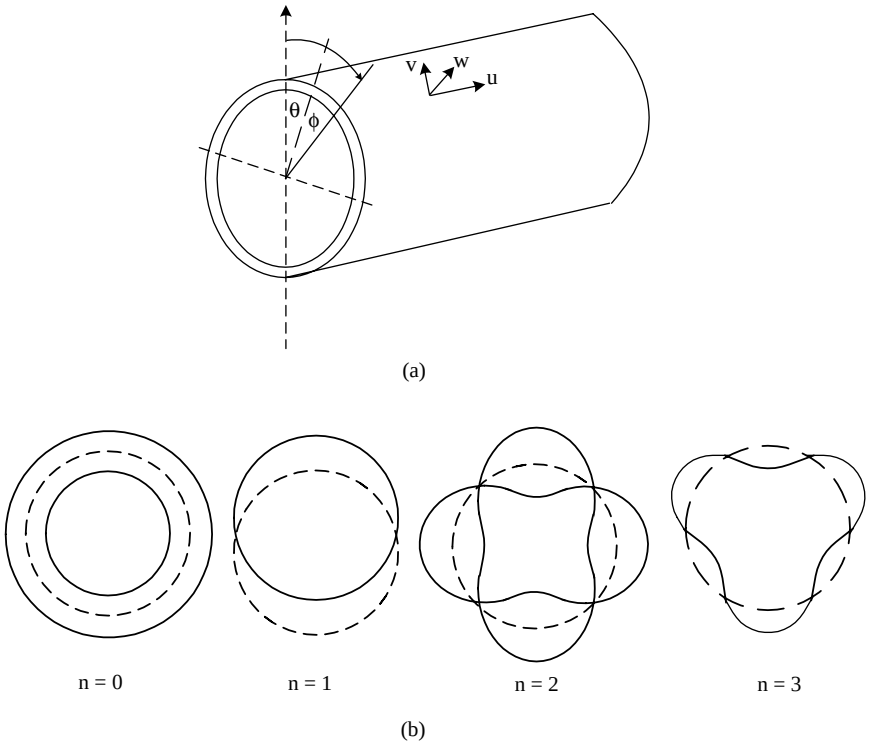

Fig. 1. Cylindrical co-ordinate system and mode shapes of a pipe.

the twisting moments. Integrating Eq. (1) in the axial direction from $-\epsilon$ to ϵ, where ϵ tends to zero gives

$$V_s|_{s=0} = \frac{1}{a}F_0\delta(\theta-\phi), \tag{2}$$

where $V_s = (Q_s + (1/a)\partial M_{s\theta}/\partial\theta)$ is called the effective transverse shear force. Since $\delta(\theta-\phi) = (1/2\pi)\sum_{n=0}^{\infty}\varepsilon_n\cos[n(\theta-\phi)]$ where n is the circumferential mode number, and $\varepsilon_n = 1$ for n = 0 and $\varepsilon_n = 2$ for $n \geqslant 1$ [14], the term on the right-hand side of Eq. (2) is the generalized force for any angle, θ. If the pipe is split at the excitation position, $s = 0$, the resultant forces and moments react at the edges of the split pipe as shown in Fig. 3. For the pipe section to the right of the excitation force, the work done by the external force, $F_0w^+/2$, is equal to that by the internal force, which is equal to the external force for the left-hand pipe section. Note that superscripts $^-$ and $^+$ denote variables for the left and right sections of the pipe, respectively. Equating the work done by the internal forces for both sections of the pipe from angle θ_1 to θ_2 gives [3]

$$\int_{\theta_1}^{\theta_2}\left[(N_s^+u^+ - N_s^-u^-) + (T_{s\theta}^+v^+ - T_{s\theta}^-v^-) + (V_s^+w^+ + V_s^-w^-) - \frac{1}{a}\left(M_s^+\frac{\partial w^+}{\partial s} - M_s^-\frac{\partial w^-}{\partial s}\right)\right]a\,\mathrm{d}\theta$$
$$-(M_{s\theta}^+w^+ - M_{s\theta}^-w^-)|_{\theta_1}^{\theta_2} = 0, \tag{3}$$

where N_s is the normal axial in-plane force, $T_{s\theta}^+ = \mathrm{N}_{s\theta}^+ + (1/a)M_{s\theta}^+$ is called the effective in-plane shear force and $\mathrm{N}_{s\theta}$ is the in-plane shear force. Eq. (3) is satisfied if the integral and the second

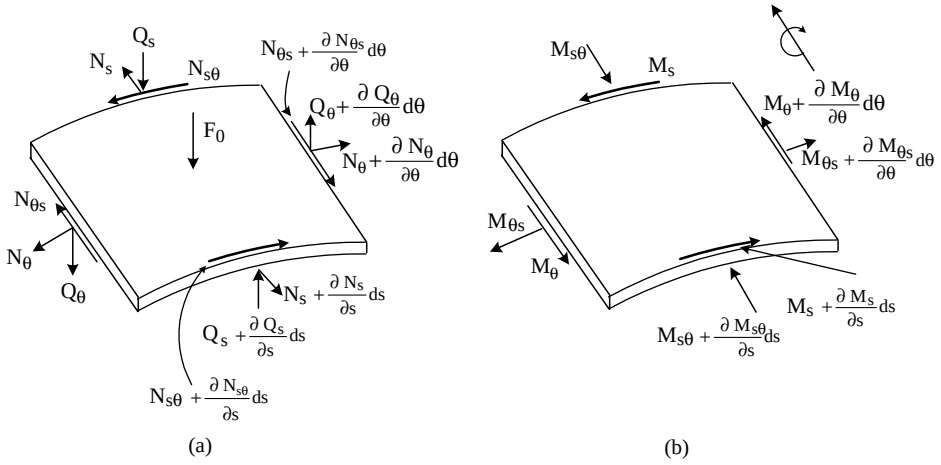

Fig. 2. Notation and co-ordinate system for an element of a pipe.

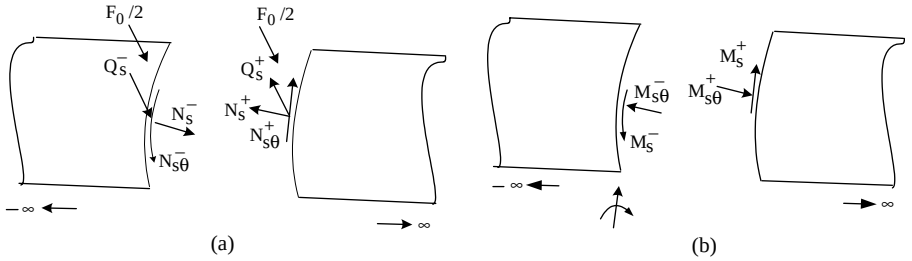

Fig. 3. Notation and co-ordinate system for two connecting pipe elements. (a) force, (b) moment.

term are both zero, which leads to the following boundary conditions at $s = 0$:

$$N_s^+ = N_s^-, \tag{4a}$$

$$T_{s\theta}^+ = T_{s\theta}^-, \tag{4b}$$

$$\mathrm{V_s^+} = -V_s^-, \tag{4c}$$

$$\mathrm{M_s^+} = M_s^-. \tag{4d}$$

For continuity of motion, the other boundary conditions are

$$u^+ = u^-, \tag{5a}$$

$$\upsilon^+ = \upsilon^-, \tag{5b}$$

$$w^+ = w^-, \tag{5c}$$

$$\frac{\partial w^+}{\partial s} = \frac{\partial w^-}{\partial s}. \tag{5d}$$

Using Flügge's shell theory [15,16], the forces and moments in Eq. (4) may be written in terms of displacements as

$$N_s^+ = \frac{K}{a}\left[\frac{\partial u^+}{\partial s} + \nu\frac{\partial \upsilon^+}{\partial \theta} + \left(\nu - \beta^2\frac{\partial^2}{\partial s^2}\right)w^+\right], \tag{6a}$$

$$T_{s\theta}^+ = \frac{(1-\nu)K}{2a}\left[\frac{\partial u^+}{\partial \theta} + (1+3\beta^2)\frac{\partial \upsilon^+}{\partial s} - 3\beta^2\frac{\partial^2 w^+}{\partial s\partial\theta}\right], \tag{6b}$$

$$V_s^+ = \frac{D}{a^3}\left[\left(\frac{\partial^2}{\partial s^2} - \frac{(1-\nu)}{2}\frac{\partial^2}{\partial\theta^2}\right)u^+ + \frac{(3-\nu)}{2}\frac{\partial^2 \upsilon^+}{\partial s\partial\theta} - \left(\frac{\partial^3}{\partial s^3} + (2-\nu)\frac{\partial^3}{\partial s\partial\theta^2}\right)w^+\right], \tag{6c}$$

$$M_s^+ = \frac{D}{a^2}\left[\frac{\partial u^+}{\partial s} + \nu\frac{\partial \upsilon^+}{\partial \theta} - \left(\frac{\partial^2}{\partial s^2} + \nu\frac{\partial^2}{\partial\theta^2}\right)w^+\right], \tag{6d}$$

where $K = Eh/(1-\nu^2)$ is the membrane stiffness, $D = Eh^3/12(1-\nu^2)$ is the bending stiffness, $\beta = h/a\sqrt{12}$, and E and ν are Young's modulus and the Poisson ratio of the pipe, respectively. Since the boundary conditions at the edges of the split pipe involve displacements in the axial, circumferential and radial directions, the relationships between them need to be determined, before their amplitudes can be established. The displacements of an infinite pipe in the positive direction are given by [13]

$$u^+(s,\theta,t) = \sum_{n=0}^{\infty}\sum_{b=1}^{4}\bar{\bar{U}}_{nb}\cos[n(\theta-\phi)]e^{j(\hat{k}_{nb}s-\pi/2-\omega t)}, \tag{7a}$$

$$\upsilon^+(s,\theta,t) = \sum_{n=0}^{\infty}\sum_{b=1}^{4}\bar{\bar{V}}_{nb}\sin[n(\theta-\phi)]e^{j(\hat{k}_{nb}s-\omega t)}, \tag{7b}$$

$$w^+(s,\theta,t) = \sum_{n=0}^{\infty}\sum_{b=1}^{4}\bar{\bar{W}}_{nb}\cos[n(\theta-\phi)]e^{j(\hat{k}_{nb}s-\omega t)}, \tag{7c}$$

where $j = \sqrt{-1}$, $\hat{k}_{nb}$ is the non-dimensional axial wavenumber (the axial wavenumber multiplied by the radius of the pipe), and $\bar{\bar{U}}_{nb}$, $\bar{\bar{V}}_{nb}$, $\bar{\bar{W}}_{nb}$ are the axial, circumferential, and radial amplitudes for the bth wave of the nth circumferential mode of the pipe, respectively. The axial and tangential motions can be found in terms of the radial motion by [15,16]

$$\begin{bmatrix} L_{11}L_{12} \\ L_{21}L_{22} \end{bmatrix}\begin{bmatrix} \bar{\bar{U}}_{nb} \\ \bar{\bar{V}}_{nb} \end{bmatrix} = -\begin{bmatrix} L_{13} \\ L_{23} \end{bmatrix}\bar{\bar{W}}_{nb}, \tag{8}$$

where

$$L_{11} = \hat{k}_{nb}^2 + \frac{(1-\nu)}{2}(1+\beta^2)n^2 - \Omega^2, \quad L_{12} = \frac{(1+\nu)}{2}n\hat{k}_{nb}, \quad L_{13} = \nu\hat{k}_n + \beta^2\hat{k}_n^3 - \frac{(1-\nu)}{2}\beta^2 n^2\hat{k}_{nb},$$

$$L_{21} = L_{12}, \quad L_{22} = \frac{(1-\nu)}{2}(1+3\beta^2)\hat{k}_{nb}^2 + n^2 - \Omega^2, \quad L_{23} = n + \frac{(3-\nu)}{2}\beta^2 n\hat{k}_{nb}^2,$$

$\Omega = \omega/\omega_r$ is the frequency normalised to the ring frequency, which is given by $\omega_r = 1/a\sqrt{E/\rho(1-\nu^2)}$. Rearranging Eq. (8) gives

$$\bar{\bar{U}}_{nb} = \alpha_{nb}\bar{\bar{W}}_{nb} \tag{9a}$$

and

$$\bar{\bar{V}}_{nb} = \psi_{nb}\bar{\bar{W}}_{nb}, \tag{9b}$$

where

$$\alpha_{nb} = \left(\frac{L_{12}L_{23} - L_{22}L_{13}}{L_{11}L_{22} - L_{12}L_{21}}\right)_{nb} \tag{9c}$$

and

$$\psi_{nb} = \left(\frac{L_{21}L_{13} - L_{11}L_{23}}{L_{11}L_{22} - L_{12}L_{21}}\right)_{nb} \tag{9d}$$

Omitting the term $e^{-j\omega t}$ for simplification, the set of the boundary conditions at $s = 0$ can be rewritten as a function of the radial motion by substituting the displacements given in Eq. (7) and their relationships obtained from Eq. (9a) and (9b) into Eq. (6) for the resultant forces and moments, and into Eq. (5) for continuity of motion. For a particular mode n this gives

$$(N_s^+)_n = \frac{K}{a}\sum_{b=1}^{4} Z_{N,nb}\bar{\bar{W}}_{nb}\cos[n(\theta-\phi)], \quad (T_{s\theta}^+)_n = j\frac{(1-\nu)K}{2a}\sum_{b=1}^{4} Z_{T,nb}\bar{\bar{W}}_{nb}\sin[n(\theta-\phi)],$$

$$(V_s^+)_n = j\frac{D}{a^3}\sum_{b=1}^{4} Z_{V,nb}\bar{\bar{W}}_{nb}\cos[n(\theta-\phi)], \quad (M_s^+)_n = \frac{D}{a^2}\sum_{b=1}^{4} Z_{M,nb}\bar{\bar{W}}_{nb}\cos[n(\theta-\phi)],$$

$$U_n^+(s=0,\theta) = -j\sum_{b=1}^{4}\alpha_{nb}\bar{\bar{W}}_{nb}\cos[n(\theta-\phi)], \quad V_n^+(s=0,\theta) = \sum_{b=1}^{4}\psi_{nb}\bar{\bar{W}}_{nb}\sin[n(\theta-\phi)],$$

$$W_n^+(s=0,\theta) = \sum_{b=1}^{4}\bar{\bar{W}}_{nb}\cos[n(\theta-\phi)], \quad \frac{\partial W_n^+(s=0,\theta)}{\partial s} = j\sum_{b=1}^{4}\hat{k}_{nb}\bar{\bar{W}}_{nb}\cos[n(\theta-\phi)], \tag{10}$$

where, U_n^+, V_n^+, W_n^+ are the axial, circumferential and radial displacements of the nth circumferential mode, respectively, and the Z's are given by

$$Z_{N,nb} = [\hat{k}_{nb}\alpha_{nb} + \nu n\psi_{nb} + \beta^2\hat{k}_{nb}^2 + \nu], \tag{11a}$$

$$Z_{T,nb} = [n\alpha_{nb} + (1+3\beta^2)\hat{k}_{nb}\psi_{nb} + 3\beta^2 n\hat{k}_{nb}], \tag{11b}$$

$$Z_{M,nb} = [\hat{k}_{nb}\alpha_{nb} + \nu n\psi_{nb} + \hat{k}_{nb}^2 + \nu n^2], \tag{11c}$$

$$Z_{V,nb} = \left[\left(\hat{k}_{nb}^2 - \left(\frac{1-\nu}{2}\right)n^2\right)\alpha_{nb} + \left(\frac{3-\nu}{2}\right)n\hat{k}_{nb}\psi_{nb} + \hat{k}_{nb}(\hat{k}_{nb}^2 + (2-\nu)n^2)\right]. \tag{11d}$$

The relationships between the radial displacement amplitudes in the positive and negative directions are determined by applying the boundary conditions at the edges of the split pipe

to give

$$(N_s^+)_n = (N_s^-)_n, \quad (V_s^+)_n = -(V_s^-)_n, \quad (M_s^+)_n = (M_s^-)_n \quad \text{and} \quad (T_{s\theta}^+)_n = (T_{s\theta}^+)_n = 0,$$
$$V_n = V_n^+ = V_n^-, \quad W_n = W_n^+ = W_n^-, \quad U_n = U_n^+ = U_n^- = 0$$
$$\text{and} \quad \frac{\partial W_n}{\partial s} = \frac{\partial W_n^+}{\partial s} = \frac{\partial W_n^-}{\partial s} = 0. \tag{12}$$

Since $(T_{s\theta}^+)_n = 0$, with zero slope and no axial displacement it implies that at the point of excitation there is no twist,

$$\frac{\partial V_n}{\partial s} = \frac{\partial V_n^+}{\partial s} = \frac{\partial V_n^-}{\partial s} = 0. \tag{13}$$

From the conditions, $U_n = 0$, $\partial W_n/\partial s = 0$, $\partial V_n/\partial s = 0$, the effective transverse shear force, V_s, given in Eq. (6c) becomes

$$V_s^+ = \frac{D}{a^3}\left(\frac{\partial^2 U_n}{\partial s^2} - \frac{\partial^3 W_n}{\partial s^3}\right) = \mathrm{j}\frac{D}{a^3}\sum_{n=0}^{\infty}\sum_{b=1}^{4}(\hat{k}_{nb}^2\alpha_{nb} + \hat{k}_{nb}^3)\bar{\bar{W}}_{nb}\, cos[n(\theta-\phi)]. \tag{14}$$

Thus, the wave amplitudes can easily be determined by using Eq. (2), in which half of the excitation force is applied to the right-hand section of the pipe as follows:

$$V_s^+|_{s=0} = \frac{1}{2a}F_0\delta(\theta-\phi). \tag{15}$$

Substituting for V_s^+ from Eq. (14) and for $\delta(\theta-\phi) = (1/2\pi)\sum_{n=0}^{\infty}\varepsilon_n \cos[n(\theta-\phi)]$ into Eq. (15) yields the relationship between the radial amplitudes of the waves and the excitation force for a particular mode

$$\sum_{b=1}^{4}(\hat{k}_{nb}^2\alpha_{nb} + \hat{k}_{nb}^3)\bar{\bar{W}}_{nb} = -j\frac{a^2}{4\pi D}F_o\varepsilon_n. \tag{16}$$

The wave amplitudes can be determined by applying the boundary conditions at $s = 0$, which are $U_n = 0$, $\partial W_n/\partial s = 0$, $(1/n)\partial V_n/\partial s = 0$, and by using force equilibrium, $V_s^+|_{s=0} = (1/2a)F_0\delta(\theta-\phi)$. By expressing these conditions in terms of the radial displacement, which are given in Eq. (10) and (16) yields the matrix equation

$$\begin{bmatrix} \alpha_{n1} & \alpha_{n2} & \alpha_{n3} & \alpha_{n4} \\ \hat{k}_{n1} & \hat{k}_{n2} & \hat{k}_{n3} & \hat{k}_{n4} \\ \dfrac{\hat{k}_{n1}\psi_{n1}}{n} & \dfrac{\hat{k}_{n2}\psi_{n2}}{n} & \dfrac{\hat{k}_{n3}\psi_{n3}}{n} & \dfrac{\hat{k}_{n4}\psi_{n4}}{n} \\ \hat{k}_{n1}^2\alpha_{n1} + \hat{k}_{n1}^3 & \hat{k}_{n2}^2\alpha_{n2} + \hat{k}_{n2}^3 & \hat{k}_{n3}^2\alpha_{n3} + \hat{k}_{n3}^3 & \hat{k}_{n4}^2\alpha_{n4} + \hat{k}_{n4}^3 \end{bmatrix} \begin{bmatrix} \bar{\bar{W}}_{n1} \\ \bar{\bar{W}}_{n2} \\ \bar{\bar{W}}_{n3} \\ \bar{\bar{W}}_{n4} \end{bmatrix} = \begin{bmatrix} 0 \\ 0 \\ 0 \\ -\mathrm{j}\dfrac{\varepsilon_n a^2 F_0}{4\pi D} \end{bmatrix}. \tag{17}$$

Substituting for α_{nb} and ψ_{nb} from Eqs. (9c) and (9d) respectively yields the wave receptances (wave amplitude/unit force) for the nth circumferential mode

$$\Re_{n1} = \frac{-\mathrm{j}\varepsilon_n a^2(L_{11}L_{22} - L_{12}L_{21})_{n1}}{2\pi D(1-\nu)(1+3\beta^2)(1-\beta^2)(\hat{k}_{n1}^2 - \hat{k}_{n2}^2)(\hat{k}_{n1}^2 - \hat{k}_{n3}^2)(\hat{k}_{n1}^2 - \hat{k}_{n4}^2)\hat{k}_{n1}}, \tag{18a}$$

$$\Re_{n2} = \frac{-j\varepsilon_n a^2 (L_{11}L_{22} - L_{12}L_{21})_{n2}}{2\pi D(1-\nu)(1+3\beta^2)(1-\beta^2)(\hat{k}_{n2}^2 - \hat{k}_{n1}^2)(\hat{k}_{n2}^2 - \hat{k}_{n3}^2)(\hat{k}_{n2}^2 - \hat{k}_{n4}^2)\hat{k}_{n2}}, \tag{18b}$$

$$\Re_{n3} = \frac{-j\varepsilon_n a^2 (L_{11}L_{22} - L_{12}L_{21})_{n3}}{2\pi D(1-\nu)(1+3\beta^2)(1-\beta^2)(\hat{k}_{n3}^2 - \hat{k}_{n1}^2)(\hat{k}_{n3}^2 - \hat{k}_{n2}^2)(\hat{k}_{n3}^2 - \hat{k}_{n4}^2)\hat{k}_{n3}}, \tag{18c}$$

$$\Re_{n4} = \frac{-j\varepsilon_n a^2 (L_{11}L_{22} - L_{12}L_{21})_{n4}}{2\pi D(1-\nu)(1+3\beta^2)(1-\beta^2)(\hat{k}_{n4}^2 - \hat{k}_{n1}^2)(\hat{k}_{n4}^2 - \hat{k}_{n2}^2)(\hat{k}_{n4}^2 - \hat{k}_{n3}^2)\hat{k}_{n4}}. \tag{18d}$$

The corresponding negative-going waves are equal to the positive-going waves because of symmetry. For the $n = 0$ mode, $\Re_{02} = 0$ because it is a torsional wave and is not excited by a radial force due to symmetry [17]. The mobility is found by summing the wave receptances and differentiating with respect to time to give

$$Y_n(s,\theta) = -j\omega \sum_{b=1}^{4} \Re_{nb} \cos[n(\theta - \phi)] e^{j\hat{k}_{nb}s}. \tag{19}$$

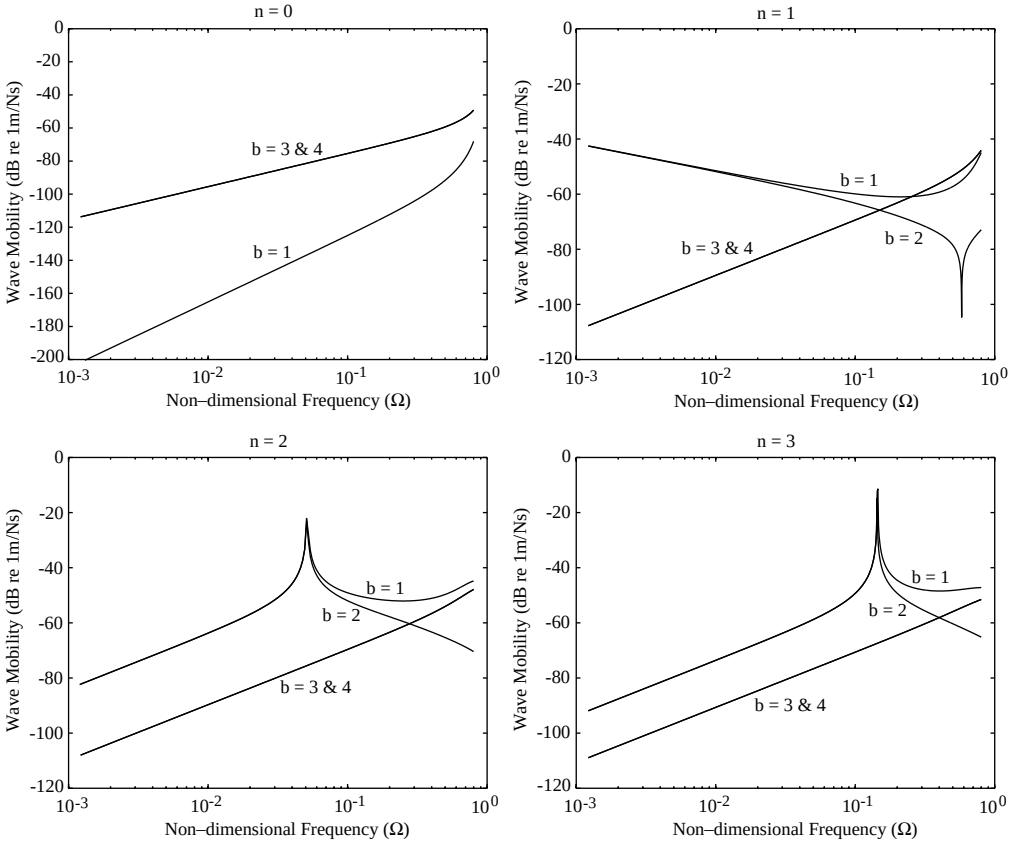

Fig. 4. Wave mobility of the modes $n = 0-3$ of the infinite pipe.

Table 1
Properties of a PVC pipe

E (N/m^2)	ρ (kg/m^3)	ν	a (mm)	h (mm)	η
3.974×10^9	1460	0.33	33.2	2.2	0.035

In Fig. 4, the individual wave mobilities for circumferential modes $n = 0$, 1, 2, and 3 for an undamped pipe are plotted against non-dimensional frequencies from 0.0012 to 0.8, which corresponds to the frequency range 10–6.7 kHz for the pipe data given in Table 1. It can be seen for the $n = 0$ mode that the standing nearfield waves, $b = 3$ and 4, dominate the response of the pipe at the excitation point. However, these waves decay away rapidly from the source. In the far field, therefore, where the amplitude of the evanescent wave generated by the point force is negligible, only the longitudinal wave, $b = 1$, contributes significantly to the radial motion of the $n = 0$ mode (the torsional wave amplitude $b = 2$ is equal to zero). It should be noted that the scale of the vertical axis for this mode is different from that for the other modes as the radial amplitude is much smaller.

For the $n = 1$ mode, the propagating ($b = 1$) and the nearfield ($b = 2$) waves dominate the response of the infinite pipe, especially at low frequencies. The effect of the standing nearfield waves, $b = 3$ and 4, increases with increasing frequency. For the $n = 2$ mode, before the waves cut on, all waves are standing nearfield waves. These waves can be separated into two groups, which have small ($b = 1$ and 2) and large ($b = 3$ and 4) wavenumbers as shown by Variyart and Brennan [13]. After the waves cut on, the standing nearfield waves with small wavenumbers disappear and the flexural ($b = 1$) wave starts to propagate. Both $b = 1$ and 2 waves dominate the pipe motion. Like the $n = 1$ mode, the standing nearfield waves influence the response of the $n = 2$ mode at high frequencies. The dynamic behaviour of the $n = 3$ mode is similar to that of the $n = 2$ mode except it has a higher cut-on frequency.

3. Approximate low-frequency mobilities

The expressions for the wave receptances derived in the previous section can be simplified by making approximations at low frequencies. When $\Omega \ll 1$, $\hat{k}_{n1}$ and $\hat{k}_{n2}$ are much smaller than $\hat{k}_{n3}$ and $\hat{k}_{n4}$, which are the standing nearfield wavenumbers, and can be ignored [13]. Also neglecting β^2 in comparison with unity, the wave receptances obtained given in Eq. (18) become

$$\mathfrak{R}_{n1} = \frac{-\mathrm{j}\varepsilon_n a^2 (L_{11}L_{22} - L_{12}L_{21})_{n1}}{2\pi D(1-\nu)\hat{k}_{n1}\hat{k}_{n3}^2\hat{k}_{n4}^2(\hat{k}_{n1}^2 - k_{n2}^2)}, \tag{20a}$$

$$\mathfrak{R}_{n2} = \frac{-\mathrm{j}\varepsilon_n a^2 (L_{11}L_{22} - L_{12}L_{21})_{n2}}{2\pi D(1-\nu)\hat{k}_{n2}\hat{k}_{n3}^2\hat{k}_{n4}^2(\hat{k}_{n2}^2 - \hat{k}_{n1}^2)}, \tag{20b}$$

$$\Re_{n3} = \frac{-j\varepsilon_n a^2 (L_{11}L_{22} - L_{12}L_{21})_{n3}}{2\pi D(1-\nu)\hat{k}_{n3}^5(\hat{k}_{n3}^2 - \hat{k}_{n4}^2)}, \tag{20c}$$

$$\Re_{n4} = \frac{-j\varepsilon_n a^2 F_0 (L_{11}L_{22} - L_{12}L_{21})_{n4}}{2\pi D(1-\nu)\hat{k}_{n4}^5(\hat{k}_{n4}^2 - \hat{k}_{n3}^2)}. \tag{20d}$$

3.1. $n = 0$ mode

Because of its distinguishable behaviour, the $n = 0$ mode is considered separately from the $n \geqslant 1$ modes. The standing nearfield waves dominate the response of the pipe at the excitation point and only the longitudinal propagating wave dominates the response in the far field, where the amplitudes of the evanescent waves generated by the point force are negligible. Hence, the point mobility of the $n = 0$ mode of an infinite pipe can be approximated by the combination of both standing nearfield waves and the transfer mobility in the far field approximated by the longitudinal propagating wave.

To simplify the mobility of the $n = 0$ mode at low frequencies the approximate wavenumbers given in Appendix A are used. In the positive direction they are given by

$$\hat{k}_{01} = -\hat{k}_l, \tag{21a}$$

$$\hat{k}_{02} = -\hat{k}_s, \tag{21b}$$

$$\hat{k}_{03} = \left[\frac{(1-\nu^2)(1-\hat{k}_l^2)}{4\beta^2}\right]^{1/4}(+1+j) \tag{21c}$$

$$\hat{k}_{04} = \left[\frac{(1-\nu^2)(1-\hat{k}_l^2)}{4\beta^2}\right]^{1/4}(-1+j) \tag{21d}$$

where $\hat{k}_l$ and $\hat{k}_s$ are the non-dimensional longitudinal and torsional wavenumbers respectively. Substituting for $(L_{11}L_{22} - L_{12}L_{21})_{0b} = (\hat{k}_{0b}^2 - \Omega^2)\left[\frac{1}{2}(1-\nu)(1+3\beta^2)\hat{k}_{0b}^2 - \Omega^2\right]$ together with the bending stiffness, $D = Eh^3/12(1-\nu^2)$, and wavenumbers into Eq. (20a) yields the expression for the $\Re_{01}$ wave:

$$\Re_{01} = \frac{j\nu^2\hat{k}_l}{4\pi K(1-\nu^2)(1-\hat{k}_l^2)}. \tag{22a}$$

In addition to the assumption of a very small longitudinal wave amplitude at low frequencies, for the standing nearfield waves, $\hat{k}_{03}^2, \hat{k}_{04}^2 \gg \Omega^2$ can also be assumed. Hence, the standing nearfield waves become

$$\Re_{03} = \frac{-j}{8\pi\beta^2 K\hat{k}_{03}^3}, \tag{22b}$$

$$\Re_{04} = \frac{-j}{8\pi\beta^2 K\hat{k}_{04}^3}. \tag{22c}$$

As mentioned in the previous section, the wave receptance of the torsional wave, $\mathfrak{R}_{02}$, is zero for the $n=0$ mode. By combining the wave mobilities the mobility of the $n=0$ is found to be

$$Y_0(s,\theta) = -\mathrm{j}\omega[\mathfrak{R}_{01}\mathrm{e}^{\mathrm{j}\hat{k}_{01}s} + \mathfrak{R}_{03}\mathrm{e}^{\mathrm{j}\hat{k}_{03}s} + \mathfrak{R}_{04}\mathrm{e}^{\mathrm{j}\hat{k}_{04}s}]. \tag{23}$$

Because the standing nearfield waves dominate the motion of the infinite pipe at the excitation point, the approximate point mobility is given by

$$Y_0^P = -\mathrm{j}\omega(\mathfrak{R}_{03} + \mathfrak{R}_{04}) = -\frac{(1+\mathrm{j})\omega}{8\pi\beta^2 K\hat{k}_{03}^3}. \tag{24}$$

The approximate transfer mobility in the far field is dominated by the longitudinal propagating wave and is thus given by

$$Y_0^T(s,\theta) = -\mathrm{j}\omega\mathfrak{R}_{01} = \frac{\omega v^2\hat{k}_l}{4\pi K(1-v^2)(1-\hat{k}_l^2)}\mathrm{e}^{-\mathrm{j}\hat{k}_l s}. \tag{25}$$

3.2. $n \geqslant 1$ modes

The standing nearfield wave receptances for the $n \geqslant 1$ modes are much smaller than the propagating and nearfield waves at low frequencies. Therefore, the point mobility is dominated by the propagating and nearfield waves. In the far field, however, the mobility is dominated by the propagating wave. To simplify these mobility expressions for low frequencies it is assumed that $\beta^2 \ll 1$ and $\hat{k}_{nb}^2 \gg \Omega^2$. The latter assumption is because the propagating wavenumber rapidly increases after the wave cuts on. Applying these assumptions gives $(L_{11}L_{22} - L_{12}L_{21})_{nb} \cong \frac{1}{2}(1-v)(n^2+\hat{k}_{nb}^2)^2$ which is substituted into Eq. (20a) and (20b) to give

$$\mathfrak{R}_{n1} = \frac{-\mathrm{j}a^2(n^2+\hat{k}_{n1}^2)^2}{2\pi D\hat{k}_{n1}\hat{k}_{n3}^2\hat{k}_{n4}^2(\hat{k}_{n1}^2-\hat{k}_{n2}^2)}, \tag{26a}$$

$$\mathfrak{R}_{n2} = \frac{-\mathrm{j}a^2(n^2+\hat{k}_{n2}^2)^2}{2\pi D\hat{k}_{n2}\hat{k}_{n3}^2\hat{k}_{n4}^2(\hat{k}_{n2}^2-\hat{k}_{n1}^2)}. \tag{26b}$$

The expression for the mobility then becomes

$$Y_n(s,\theta) = -\mathrm{j}\omega\cos[n(\theta-\phi)][\mathfrak{R}_{n1}\mathrm{e}^{\mathrm{j}\hat{k}_{n1}s} + \mathfrak{R}_{n2}\mathrm{e}^{\mathrm{j}\hat{k}_{n2}s}]. \tag{27}$$

This yields the point mobility

$$Y_n^P = -\mathrm{j}\omega(\mathfrak{R}_{n1} + \mathfrak{R}_{n2}) = -\frac{a^2}{2\pi D\hat{k}_{n3}^2\hat{k}_{n4}^2(\hat{k}_{n1}^2-\hat{k}_{n2}^2)}\left[\frac{(n^2+\hat{k}_{n1}^2)^2}{\hat{k}_{n1}} - \frac{(n^2+\hat{k}_{n2}^2)^2}{\hat{k}_{n2}}\right] \tag{28}$$

and the transfer mobility in the far field

$$Y_n^T(s,\theta) = -\mathrm{j}\omega\mathfrak{R}_{n1} = -\frac{a^2(n^2+\hat{k}_{n1}^2)^2}{2\pi D\hat{k}_{n1}\hat{k}_{n3}^2\hat{k}_{n4}^2(\hat{k}_{n1}^2-\hat{k}_{n2}^2)}\cos[n(\theta-\phi)]\mathrm{e}^{\mathrm{j}\hat{k}_{nb}s}. \tag{29}$$

In the case of the $n=1$ mode, the flexural ($\hat{k}_{11}$) and nearfield ($\hat{k}_{12}$) wavenumbers, are similar to those of a Timoshenko beam given in Appendix A, which results in the following wave

receptances:

$$\mathfrak{R}_{11} = -\frac{\mathrm{j}(1+\hat{k}_{11}^2)}{4\pi h E \hat{k}_b^2 \hat{k}_{11}} \tag{30a}$$

$$\mathfrak{R}_{12} = \frac{\mathrm{j}(1+\hat{k}_{12}^2)}{4\pi h E \hat{k}_b^2 \hat{k}_{12}}, \tag{30b}$$

where $\hat{k}_b$ is the non-dimensional Euler–Bernoulli bending wavenumber. Substituting for the wave amplitudes from Eq. (30) into Eq. (27) gives the approximate mobility of this mode. When $\Omega^2 \ll 1$ and $\hat{k}_b^2 \gg \hat{k}_b^4, \hat{k}_l^2, \hat{k}_s^2$, the flexural and nearfield wavenumbers can be approximated as $\hat{k}_{11} = -\hat{k}_b$ and $\hat{k}_{12} = \mathrm{j}\hat{k}_b$. Using these approximations and setting $\hat{k}_b^2 \ll 1$ so that $\hat{k}_b^4$ can be neglected, the flexural and nearfield waves become

$$\mathfrak{R}_{11} = \frac{\mathrm{j}(1+2\hat{k}_b^2)}{4\pi h E \hat{k}_b^3}, \tag{31a}$$

$$\mathfrak{R}_{12} = \frac{(1-2\hat{k}_b^2)}{4\pi h E \hat{k}_b^3}. \tag{31b}$$

Thus, the point mobility for the $n = 1$ mode is given by

$$Y_1^P = \frac{\omega[(1-\mathrm{j}) + 2\hat{k}_b^2(1+\mathrm{j})]}{4\pi h E \hat{k}_b^3} \tag{32}$$

and the transfer mobility for this mode is given by

$$Y_1^T(s,\theta) = \frac{\omega(1+2\hat{k}_b^2)}{4\pi h E \hat{k}_b^3} \cos[n(\theta-\phi)] \mathrm{e}^{\mathrm{j}\hat{k}_b s} \tag{33}$$

At very low frequencies, the flexural wavenumber tends to zero, which means that the term containing $\hat{k}_b^2$ in the numerator of Eqs. (32) and (33) can be neglected and the mobility of the $n = 1$ mode becomes that of an Euler–Bernoulli beam.

3.3. Evaluation of the simplified mobilities

The low-frequency point and transfer mobilities are validated by comparing them with the mobilities calculated using the original model given in Eq. (19). Figs. 5 and 6 depict the point and transfer mobilities for the first four circumferential modes respectively. To ensure that the evanescent wave is sufficiently small in the far field, the transfer mobility is calculated at the non-dimensional distance $s = 100$. It should be noted that the scale for the $n = 0$ mode in Fig. 6 is larger than for the other modes.

From Figs. 5 and 6, it can be seen that, in general, the approximations give reasonably good results up to quite high frequencies. The simplification of the mobility expressions depends on there only being a small contribution to the radial motion from the waves that are neglected. It is clear that the mobility of the $n = 1$ mode simplifies to a Timoshenko beam-like model over a wide frequency range, but the Euler–Bernoulli beam-like model is only valid at relatively low

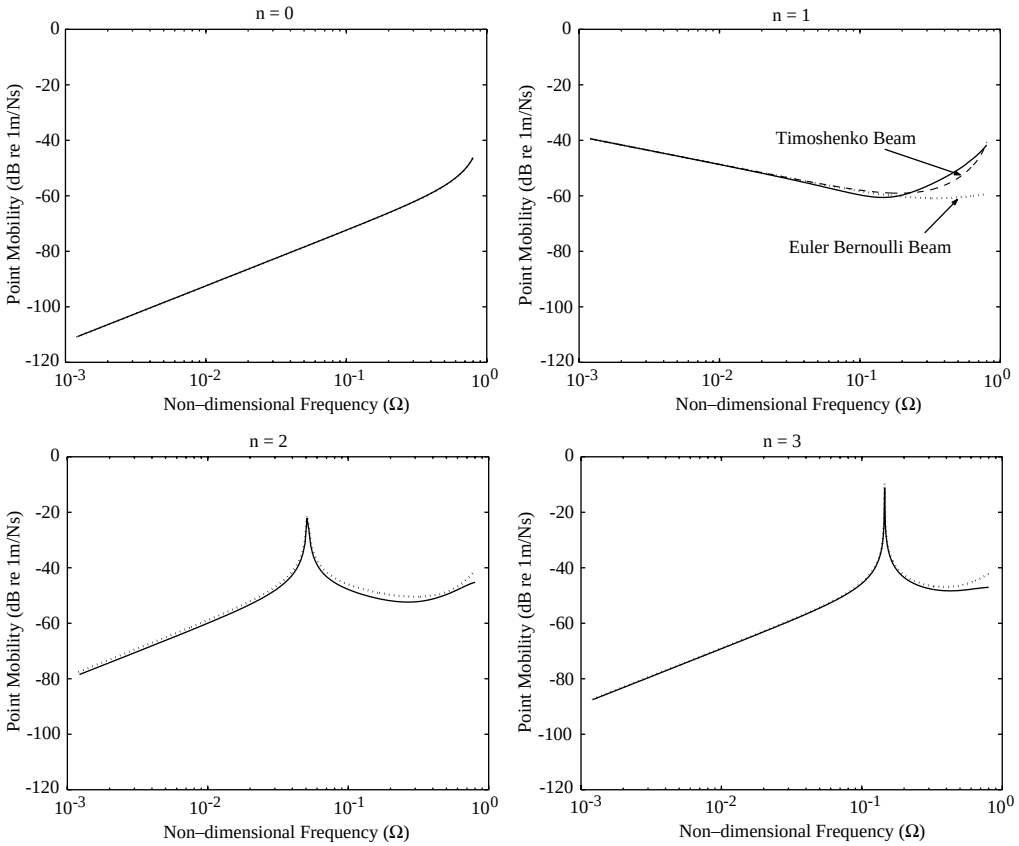

Fig. 5. Point mobility of the $n = 0-3$ modes of an infinite pipe, _, analytical method (Eq. (19)); …, simplification at low frequencies (Eq. (24) for the $n = 0$ mode, Eq. (32) for the $n = 1$ mode modelled as a Timoshenko beam, and Eq. (28) for the $n \geqslant 2$ modes).

frequencies where the flexural and nearfield waves dominate. Table 2 gives a summary of the approximate mobility formulae derived.

4. Experimental validation

To validate the transfer mobility expressions derived in the previous sections some experimental work was carried out. The experimental set-up is shown in Fig. 7. A 4.6 m long PVC pipe, whose properties are given in Table 1, was suspended by cords and fitted with anechoic terminations at both free ends in order to make the pipe behave as if it had infinite length. These terminations were wooden boxes containing sand. A random signal from an HP 3566A Signal Analyzer was supplied to the shaker, onto which a PZT element was attached with the sensitivity of 341.7 pC/N, for use as a force gauge. A PZT element was used as the force sensor because it is very light and inexpensive. The pipe was excited at its mid-point and a set of 32 measurements around the pipe

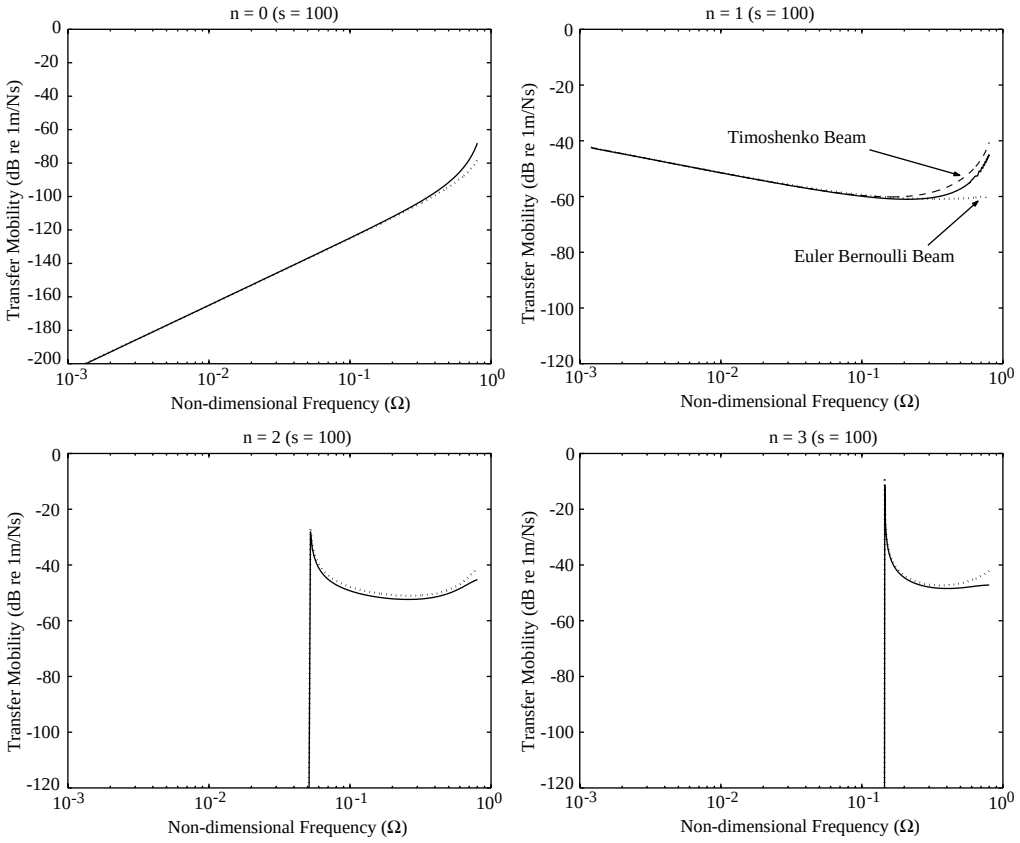

Fig. 6. Transfer mobility of the $n = 0-3$ modes of an infinite pipe, which is calculated at the distance of $s = 100$; __, analytical method (Eq. (19)); …, simplification at low frequencies (Eq. (25) for the $n = 0$ mode, Eq. (33) for the $n = 1$ mode modelled as a Timoshenko beam, and Eq. (29) for the n $\geqslant 2$ modes).

with equal angle were made at a distance of 300 mm from the shaker using a Bruel & Kjaer accelerometer type 4374, which had a mass of 0.65 g. A distance of 300 mm was chosen so that the radial acceleration of the pipe comprised all wave types. Using the modal decomposition technique described in Appendix B, the responses of each mode were extracted from the measured frequency response functions. All measured frequency response functions were accelerance, which were converted to mobility by dividing by $j\omega$. These are compared with the predictions in Fig. 8. Measured and predicted mobilities of the pipe are also compared for various azimuthal angles. To make the comparison with the experimental results the complex elastic modulus of the pipe, $E' = E(1 + j\eta)$ where η is the loss factor, was used in the predictions because of structural damping in the pipe. Before this comparison could be done, however, the reference angle (ϕ) of the pipe had to be determined, and the way in which this was obtained is described in Appendix B.

In Fig. 8(a), it can be seen that the mobility of the $n = 0$ mode calculated using Eq. (23) is very small, especially at low frequencies. It was difficult to detect this mode using accelerometers because of a poor signal-to-noise ratio leading to an inaccurate result. Another way to detect this

Table 2
Summary of the approximate mobility of an infinite pipe

Mode	Mobility	
	Point	Transfer
0	$-\dfrac{(1+\mathrm{j})\omega}{8\pi\beta^2 K\hat{k}_{03}^3}$	$\dfrac{\omega v^2\hat{k}_1}{4\pi K(1-v^2)(1-\hat{k}_1^2)}$
1	$\dfrac{\omega[(1-\mathrm{j})+2\hat{k}_b^2(1+\mathrm{j})]}{4\pi hE\hat{k}_b^3}$	$\dfrac{\omega(1+2\hat{k}_b^2)}{4\pi hE\hat{k}_b^3}$
$\geqslant 2$	$-\dfrac{a^2}{2\pi D\hat{k}_{n3}^2\hat{k}_{n4}^2(\hat{k}_{n1}^2-\hat{k}_{n2}^2)}\left[\dfrac{(n^2+\hat{k}_{n1}^2)^2}{\hat{k}_{n1}}-\dfrac{(n^2+\hat{k}_{n2}^2)^2}{\hat{k}_{n2}}\right]$	$-\dfrac{a^2(n^2+\hat{k}_{n1}^2)^2}{2\pi D\hat{k}_{n1}\hat{k}_{n3}^2\hat{k}_{n4}^2(\hat{k}_{n1}^2-\hat{k}_{n2}^2)}$

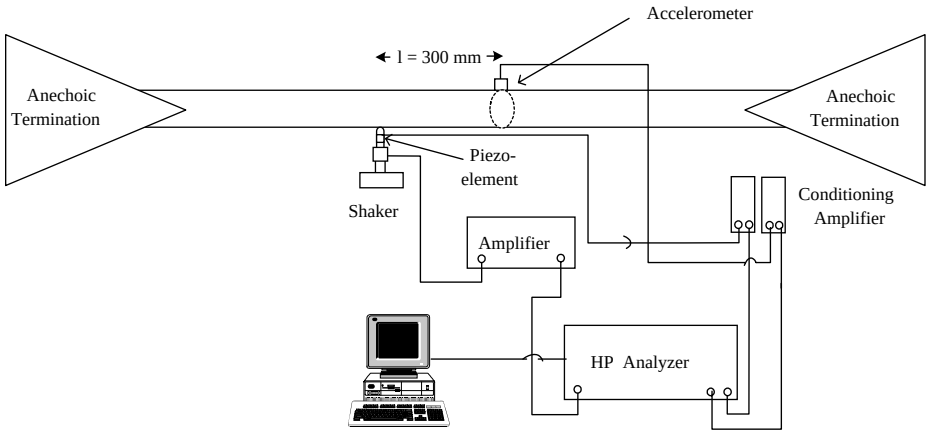

Fig. 7. Experimental set-up for the infinite pipe.

mode is to use PVDF wire, which senses strain proportional to the radial displacement of the pipe [10,18]. There is good agreement between the prediction of the $n=1$ mode modelled as a Timoshenko beam (Eq. (30)) and the experimental result as shown in Fig. 8(b). Fig. 8(c) and (d) show the consistency between the practice and the theory (Eq. (27) for $n=2$ and $n=3$ modes.

In all of the graphs, however, the effects of the higher modes are evident, especially at their cut-on frequencies. This might have been caused by inaccurate positioning of the accelerometers around the pipe or possibly large reflections from the anechoic terminations at the cut-on frequencies of the higher modes.

The reference angle, ϕ, of the acceleration measurement with respect to the force position is illustrated in Fig. 9. This angle is constant for all modes, and should be calculated in the frequency

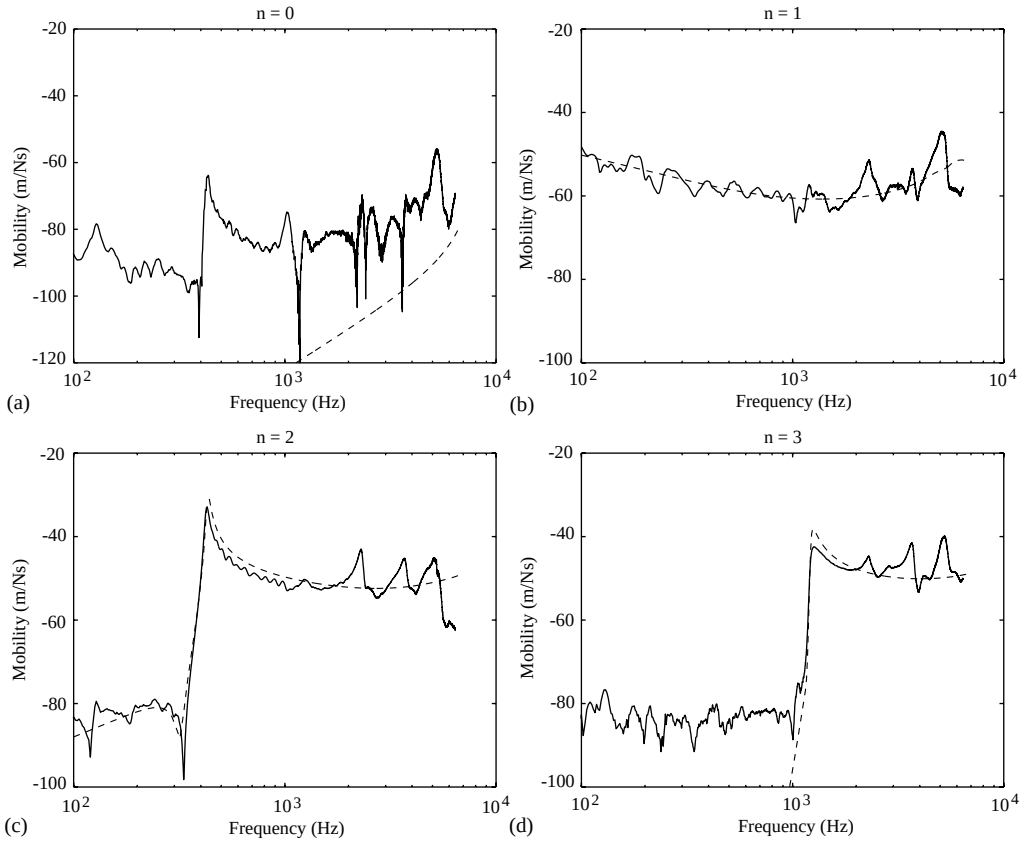

Fig. 8. Amplitude of mobility of the $n = 0-3$ modes of the infinite pipe: _, measured result; – –, prediction (Eq. (23) for the $n = 0$ mode, Eq. (33) for the $n = 1$ mode modelled as a Timoshenko beam, and Eq. (29) for the $n \geqslant 2$ modes).

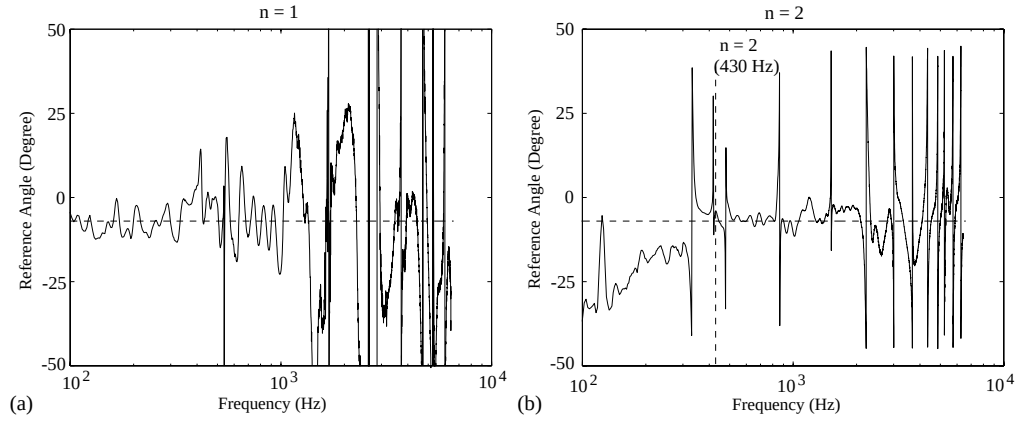

Fig. 9. Orientation angle extracted from frequency response of the $n = 1$ and $n = 2$ modes.

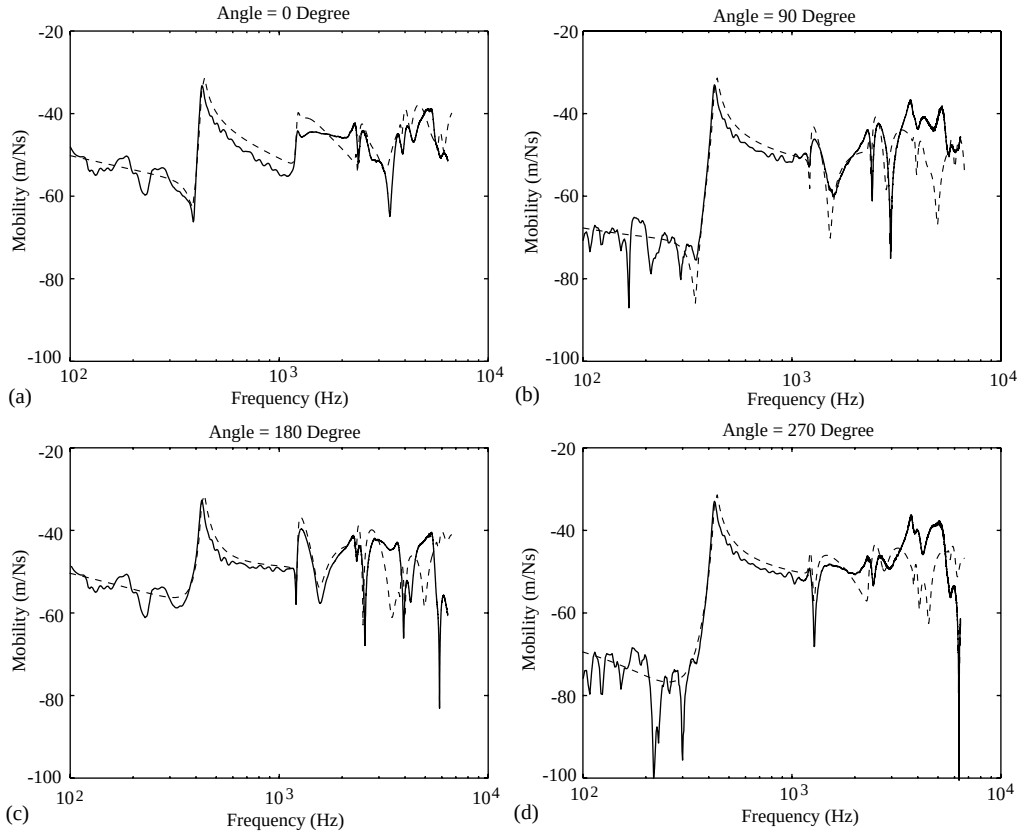

Fig. 10. Amplitude of mobility of the pipe at various angle of measurements where $\phi = -5$: __, measured result; – – prediction, which combines Eqs. (23), (29) and (33).

range where a mode has cut on but before higher modes have cut on, to improve the signal-to-noise ratio. Once the reference angle of the pipe had been determined, the mobility obtained from the experimental results could be compared with the predictions combining Eq. (23) for the $n = 0$, Eq. (33) for the $n = 1$ and Eq. (29) for the $n \geqslant 2$ modes. They are in good agreement up to high frequencies as shown in Fig. 10 for various measurement angles.

5. Conclusions

Expressions for the mobility of an infinite in vacuo pipe have been derived. This has been achieved by finding expressions for the receptances for the four wave types that can exist for each circumferential mode. These are then summed to give the modal mobilities, which can then be summed to give the total pipe mobility. In addition, simplified approximate low-frequency expressions for the point and transfer mobilities have also been derived by making assumptions about the wavenumbers and the contributions of various wave types at low frequencies. It has been shown that the simplified expressions are valid up to quite high frequencies provided that the

pipe is modelled as a Timoshenko beam for the $n = 1$ mode. The new mobility expressions have been validated by experimental work.

Appendix A. Simplified wavenumbers

This appendix summarizes the simplified low-frequency wavenumbers reported by Variyart and Brennan [13]. They are used in the approximation of the mobilities in Section 3 and are as follows.

For the $n = 0$ mode,

$$\hat{k}_{01}^2 = \hat{k}_l^2, \quad \hat{k}_{02}^2 = \hat{k}_s^2, \quad \hat{k}_{03}^2, \hat{k}_{04}^2 = \pm \mathrm{j}\sqrt{(1-\nu^2)(1-\hat{k}_l^2)/\beta^2}. \tag{A.1}$$

For the $n = 1$ mode,

$$\hat{k}_{11}^2, \hat{k}_{12}^2 = \frac{1}{2(1-\hat{k}_l^2)}[(1-\hat{k}_l^2)(\hat{k}_1^2 + \hat{k}_s^2) + \hat{k}_b^4 \pm 2\hat{k}_b^2] \quad \hat{k}_{13}^2, \hat{k}_{14}^2 = \pm \mathrm{j}\sqrt{(1-\nu^2)(1-\hat{k}_l^2)/\beta^2}. \tag{A.2}$$

For the $n \geqslant 2$ modes

$$\begin{aligned}
\hat{k}_{n1}^2 &= \frac{n^2[(\Omega^2 - 2\Omega_{co}^2) + \sqrt{(1-\nu^2+3\Omega_{co}^2)(\Omega^2-\Omega_{co}^2)+\Omega_{co}^4}]}{\beta^2 \hat{k}_{n3}^2 \hat{k}_{n4}^2}, \\
\hat{k}_{n2}^2 &= \frac{n^2[(\Omega^2 - 2\Omega_{co}^2) - \sqrt{(1-\nu^2+3\Omega_{co}^2)(\Omega^2-\Omega_{co}^2)+\Omega_{co}^4}]}{1-\nu^2-\Omega^2+6\Omega_{co}^2}, \\
\hat{k}_{n3,n4}^2 &= -n^2 + \frac{1}{6}\left[-\left(3z^{1/3} - \frac{(1-\nu^2-\Omega^2)}{\beta^2 z^{1/3}}\right) \pm \mathrm{j}\sqrt{3}\left(3z^{1/3} + \frac{(1-\nu^2-\Omega^2)}{\beta^2 z^{1/3}}\right)\right],
\end{aligned} \tag{A.3}$$

where

$$z = \left(\frac{1-\nu^2}{\beta^2}\right)\left[1 + \sqrt{1 + \frac{(1-\nu^2-\Omega^2)^3}{27(1-\nu^2)^2\beta^2 n^4}}\right] n^2, \quad \Omega_{co}^2 = \frac{\beta^2 n^2 (n^2-1)^2}{n^2+1}$$

is the cut-on frequency, $\hat{k}_l^2 = \Omega^2/1-\nu^2$, $\hat{k}_s^2 = 2\Omega^2/1-\nu$, and $\hat{k}_b^4 = 2\Omega^2/(1+3\beta^2)(1-\nu^2) \cong 2\hat{k}_l^2$ are the non-dimensional wavenumbers of longitudinal, torsional and flexural bending waves of a pipe normalized to its radius. As discussed by Variyart and Brennan [13], the flexural ($\hat{k}_{11}$) and nearfield ($\hat{k}_{12}$) wavenumbers of the $n = 1$ mode (Eq. (A.2)) are similar to those of the Timoshenko beam.

Appendix B. Modal decomposition

A point sensor such as an accelerometer placed on a pipe wall will detect all circumferential modes. To be able to detect a single mode, modal decomposition of measurements from an array of sensors is required. This technique is based on the principle of discrete orthogonality [11]. To illustrate this technique, Eq. (19) is considered. By expanding the term $\cos[n(\theta - \phi)]$ into sine and

cosine functions, this equation is written as

$$Y_n = -\mathrm{j}\omega[\lambda_1 \cos(n\theta) + \lambda_2 \sin(n\theta)] \sum_{b=1}^{4} \Re_{nb} \mathrm{e}^{\mathrm{j}\hat{k}_{nb}s}, \tag{B.1}$$

where $\Re_{nb}$ is given in Eq. (18), $\lambda_1 = \cos(n\phi)$, $\lambda_2 = \sin(n\phi)$ and ϕ is the reference angle. Since the term on the right-hand side of this equation consists of two separate parameters, θ and s, the total mobility may be written as

$$Y = \sum_{n=0}^{\infty} \varepsilon_n A_n [\lambda_1 \cos(n\theta) + \lambda_2 \sin(n\theta)], \tag{B.2}$$

where $A_n = -\mathrm{j}\,\omega/\varepsilon_n \sum_{b=1}^{4} \Re_{nb} \mathrm{e}^{\mathrm{j}\hat{k}_{nb}s}$. Assuming that the measurement is made using a point sensor at N points around a pipe with equal angle, then, $\theta = (2\pi/N)p_\theta$, where p_θ is the position of the measurement. To decompose pipe modes in terms of the cosine function, both sides of Eq. (B.2) are multiplied by $(1/N)\cos((2\pi p_\theta/N)m)$ and all responses measured around the pipe are summed to give

$$\begin{aligned} &\frac{1}{N} \sum_{p=0}^{N-1} Y \cos\left(\frac{2\pi p_\theta}{N} m\right) \\ &\quad = \frac{1}{N} \sum_{p=0}^{N-1} \sum_{n=0}^{\infty} \varepsilon_n A_n \left(\lambda_1 \cos\left(\frac{2\pi p_\theta}{N} n\right) + \lambda_2 \sin\left(\frac{2\pi p_\theta}{N} n\right)\right) \cos\left(\frac{2\pi p_\theta}{N} m\right), \end{aligned} \tag{B.3}$$

where m is the desired mode to be decomposed. Using the property of orthogonality, the response of the desired mode for the cosine function can be determined as

$$Y_n^c = \frac{1}{N} \sum_{p=0}^{N-1} Y \cos\left(\frac{2\pi p_\theta}{N} n\right) = \lambda_1 A_n, \quad m = n. \tag{B.4}$$

The term of Y_n^c is denoted for the measured mobility of the nth mode decomposed with the cosine function. To decompose pipe modes in terms of the sine function, the same procedure is applied except that both sides are multiplied by $(1/N)\sin((2\pi p_\theta/N)m)$ instead of $(1/N)\cos((2\pi p_\theta/N)m)$. Hence, the response of the desired mode for the sine function is

$$Y_n^s = \frac{1}{N} \sum_{p=0}^{N-1} Y \sin\left(\frac{2\pi p_\theta}{N} n\right) = \lambda_2 A_n, \quad m = n \tag{B.5}$$

where the term of Y_n^s is denoted for the measured mobility of the nth mode decomposed with the sine function. The total response, A_n, of the desire mode can be obtained by combining Eqs. (B.4) and (B.5) as follows to give

$$A_n = \sqrt{(Y_n^c)^2 + (Y_n^s)^2} \tag{B.6}$$

and the reference angle is obtained from

$$\phi = \frac{1}{n} \tan^{-1}\left(\frac{\lambda_2}{\lambda_1}\right) = \frac{1}{n} \tan^{-1}\left(\frac{Y_n^s}{Y_n^c}\right). \tag{B.7}$$

References

[1] A.V. Metrikine, M.V. Tochilin, Steady-state vibrations of an elastic ring under a moving load, Journal of Sound and Vibration 232 (3) (2000) 511–524.
[2] J.L. Palladino, V.H. Neubert, Mobility of a long cylindrical shell, Journal of the Acoustical Society of America 42 (2) (1967) 403–411.
[3] W. Soedel, Vibrations of Shells and Plates, 2nd Edition, Marcel Dekker, New York, 1993.
[4] S. Finnveden, Formulas for modal density and for input power from mechanical and fluid point sources in fluid filled pipes, Journal of Sound and Vibration 208 (5) (1997) 705–728.
[5] P.A. Franken, Input impedances of simple cylindrical structures, Journal of the Acoustical Society of America 32 (4) (1960) 473–477.
[6] M. Heckl, Vibrations of point-driven cylindrical shells, Journal of the Acoustical Society of America 34 (10) (1962) 1553–1557.
[7] C.F. Fuller, The input mobility of an infinite circular cylindrical elastic shell filled with fluid, Journal of Sound and Vibration 87 (3) (1983) 409–427.
[8] B.J. Brevart, C.F. Fuller, Active control of coupled wave propagation in fluid-filled elastic cylindrical shells, Journal of the Acoustical Society of America 94 (3) (1993) 1467–1475.
[9] M.B. Xu, W.H. Zhang, Vibrational power flow input and transmission in a circular cylindrical shell filled with fluid, Journal of Sound and Vibration 234 (3) (2000) 387–403.
[10] R.J. Pinnington, A.R. Briscoe, Externally applied sensor for axisymmetric waves in a fluid filled pipe, Journal of Sound and Vibration 173 (4) (1994) 503–516.
[11] G. Arfken, Mathematical Methods for Physicists, 3rd Edition, Academic Press, New York, 1985.
[12] O. Fégeant, Closed form solutions for the point mobilities of axisymmetrically excited cylindrical shells, Journal of Sound and Vibration 243 (1) (2001) 89–115.
[13] W. Variyart, M.J. Brennan, Simplified dispersion relationships for in-vacuo pipes, Journal of Sound and Vibration 256 (5) (2002) 955–967.
[14] W. Variyart, M.J. Brennan, Measurement of flexural propagating waves in pipes using shaped PVDF modal sensors, ISVR Technical Memorandum No. 847, 1999.
[15] A.W. Leissa, Vibrations of Shells, NASA SP-288, US Government Printing Office, Washington DC, 1973.
[16] W. Flügge, Stresses in Shells, 2nd Edition, Springer, Berlin, 1962
[17] J.R. Vinson, Structural Mechanics: The Behavior of Plate and Shells, Wiley, New York, 1974.
[18] M.J. Brennan, S.J. Elliott, R.J. Pinnington, A non-intrusive fluid-wave actuator and sensor pair for the active control of fluid-borne vibrations in a pipe, Smart Materials and Structures 5 (1996) 281–296.